Available online at www.sciencedirect.com
ScienceDirect
Aerospace Science and Technology 11 (2007) 155–162
Aerospace Science and Technology
www.elsevier.com/locate/aescte

Performance prediction and optimization for liquid rocket engine nozzle

Guobiao Cai [1], Jie Fang [*,2], Xu Xu [3], Minghao Liu [4]

School of Astronautics, Beijing University of Aeronautics and Astronautics, Beijing, 100083, China

Received 11 February 2006; received in revised form 31 May 2006; accepted 13 July 2006

Available online 18 September 2006

Abstract

An optimization approach, based on computational fluid dynamics methodology, is investigated for the performance prediction and optimization of liquid rocket engine nozzle. The CFD code employs implicit Lower-Upper decomposition (LU) scheme for solving the two-dimensional axisymmetric Navier–Stokes (NS) equations and species transport equations in an efficient manner. The validity of the code is demonstrated by comparing the numerical calculations with both the experimental data and previous calculations. Then the code, called by three optimization algorithms (i.e. successive quadratic programming method, genetic algorithm and interdigitation strategy) respectively, is used to design axisymmetric optimum-thrust nozzle. Results show that improvement on nozzle thrust can be obtained over that of the baseline case.

Keywords: CFD; Performance prediction; Nozzle design; Optimal design

1. Introduction

With an increasing demand for reducing the cost of space missions, researchers are forced to investigate new technologies, such as designing and optimizing the contoured nozzles. In the early years of rocket nozzle design, conical nozzles were used because the methodology for the design of efficient contoured nozzles was not available. Classical optimization procedures usually begin with an inviscid design (such as the Rao's method of design [7]), then a boundary-layer correction is added to compensate for the viscous effects. More recent advances in computational technology have allowed researchers to integrate the full NS equations, which previously had to be simplified for computation. Such advances have given rise to efficient CFD codes that have eliminated approximation in simulating the viscous effects in traditional nozzle contour design [1,4].

In this study, a liquid rocket engine nozzle is designed by using a CFD-based optimization procedure which links the well-tested CFD code to three optimization codes. Different from previous work, the investigation takes the viscous effect into account as well as the chemical reactions occurring in the nozzle. Different optimization methods get similar results. Compared with the baseline nozzle, the optimized design achieves improvements in nozzle performance.

2. Governing equations

The governing equations for a compressible viscous fluid in the absence of body forces consist of the unsteady Navier–Stocks equations. These equations can be written in conservative form as follows:

$$\frac{\partial U}{\partial t} + \frac{\partial F}{\partial x} + \frac{1}{y^{j_0}}\frac{\partial}{\partial y}\left(y^{j_0}G\right) = \frac{\partial F_v}{\partial x} + \frac{1}{y^{j_0}}\frac{\partial}{\partial y}\left(y^{j_0}G\right) + j_0\frac{H}{y^{j_0}} + S$$

where $j_0 = 0$ or 1 for either two-dimensional or axisymmetric flow respectively, and

* Corresponding author. Tel.: +86 10 82317206; fax: +86 10 82316533.
E-mail address: mdorg@buaa.edu.cn (J. Fang).
[1] Professor, School of Astronautics.
[2] PhD Student, School of Astronautics, Student Member AIAA.
[3] Professor, School of Astronautics.
[4] Graduate Research Assistant, School of Astronautics.

1270-9638/$ – see front matter
doi:10.1016/j.ast.2006.07.002

Nomenclature

A, B, Z	Jacobian matrix
A_{fi}, B_{fi}, C_{fi}	Reaction rate coefficients
A_t	Area of nozzle throat
C_f	Thrust coefficient
C_p	Constant-pressure specific heat
D	Diagonal matrices
e	Specific energy
F, G	Fluxes of mass, momentum, energy
F	Thrust
h	Specific enthalpy
I	Identity matrix
k	Chemical reaction rate
L	Lower triangular matrix
M	Molecular weight
n_r	Number of chemical reaction
n_s	Number of species
p	Pressure
q_x, q_y	Heat flux
R	Molar concentration
r_A, r_B	Eigenvalues of Jacobian
S	Source terms
T	Temperature
t	Time
U	Conserved variables, upper triangular matrix
u, v	Cartesian velocities
x, y	Cartesian coordinates
X	Molar fraction

Greek symbols

β	Coefficient of LU scheme
ζ	Performance loss coefficient
λ	Thermal conductivity
μ	Dynamic viscosity
ν	Stoichiometric coefficient
ρ	Density
τ	Stress
$\dot{\omega}$	Rate of production

Subscripts

c	Combustor
E	Euler equations
f	Friction
i	Species i
m	Mixing
N	Navier–Stokes equations
n	Chemically frozen
o	One dimensional
r	Chemical reaction
stg	Stagnation value
t	Two dimensional
x	Axial
η, ξ	Computation coordinates
ν	Viscous

Superscripts

f	Forward reaction
b	Backward reaction
n	Time level
$\pm$	Eigenvalues of matrices are non-negative or non-positive

$$U = \begin{bmatrix} \rho_i \\ \rho u \\ \rho v \\ \rho e \end{bmatrix}, \qquad F = \begin{bmatrix} \rho_i u \\ \rho u^2 + p \\ \rho uv \\ (\rho e + p)u \end{bmatrix}$$

$$G = \begin{bmatrix} \rho_i v \\ \rho uv \\ \rho v^2 + p \\ (\rho e + p)v \end{bmatrix}, \qquad F_v = \begin{bmatrix} D_{im} \frac{\partial \rho_i}{\partial x} \\ \tau_{xx} \\ \tau_{xy} \\ \tau_{xx} u + \tau_{xy} v - q_x \end{bmatrix}$$

$$G_v = \begin{bmatrix} D_{im} \frac{\partial \rho_i}{\partial y} \\ \tau_{xy} \\ \tau_{yy} \\ \tau_{xy} u + \tau_{yy} v - q_y \end{bmatrix}, \qquad H = \begin{bmatrix} 0 \\ 0 \\ p - \tau_H \\ 0 \end{bmatrix}$$

$$S = \begin{bmatrix} \omega_i \\ 0 \\ 0 \\ 0 \end{bmatrix}, \quad i = 1, \ldots, N$$

The stress and heat-transfer components are given as:

$$\tau_{xx} = \left[-\frac{2}{3}\mu \left(\frac{\partial u}{\partial x} + \frac{\partial v}{\partial y} \right) + 2\mu \frac{\partial u}{\partial x} \right]$$

$$\tau_{xy} = \mu \left(\frac{\partial u}{\partial y} + \frac{\partial v}{\partial x} \right)$$

$$\tau_{yy} = \left[-\frac{2}{3}\mu \left(\frac{\partial u}{\partial y} + \frac{\partial v}{\partial x} \right) + 2\mu \frac{\partial v}{\partial y} \right]$$

$$\tau_H = \left[-\frac{2}{3}\mu \left(\frac{\partial u}{\partial y} + \frac{\partial v}{\partial x} \right) + 2\mu \frac{v}{y} \right]$$

$$q_x = -\lambda \frac{\partial T}{\partial x} - \sum_{i=1}^{N} D_{im} h_i \frac{\partial \rho_i}{\partial x}$$

$$q_y = -\lambda \frac{\partial T}{\partial y} - \sum_{i=1}^{N} D_{im} h_i \frac{\partial \rho_i}{\partial y}$$

where $D_{im} = (1 - X_i) / \sum_{j \neq i}^{N} (X_j / D_{ij})$ is the effective binary diffusivity of species i in the gas mixture, obtained by treating the species i and the surrounding gas as a binary mixture, and X_i is the molar fraction of species i. The binary mass diffusivity D_{ij} between species i and j is obtained using the Chapman–Enskog's theory.

h_i is the specific enthalpy

$$h_i = h_{fi} + \int_{T_{\text{ref}}}^{T} c_{pi} \, \mathrm{d}T$$

where h_{fi} is the specific heat of formation, and c_{pi} is the constant pressure specific heat of species i.

Assuming that ideal gas equation is applicable to all of the species, the equation of state becomes

$$p = \sum_{i=1}^{N} \rho_i R_i T$$

The temperature is calculated from the conservative variables using the Newton's iteration method.

The above equations can be easily applied to different computational cases. For chemically frozen flow, the S is set to zero. For inviscid computation, the F_v is set to zero, as is G_v.

The Baldwin–Lomax model and the body-fitted grid system are adopted here to achieve the accurate and robust results.

3. Numerical scheme

Various numerical techniques have been used to solve the set of equations governing chemically reacting flows. Among these techniques, explicit schemes are generally slow to converge when the flow involves violent chemical reactions and heat release. Most implicit schemes, on the other hand, require the inversion of banded block matrices and become exceedingly expensive when the chemical system involves a large number of species. In the present study, the LU [8,9] scheme is adopted to solve the two-dimensional axisymmetric Navier–Stokes and species transport equations. In this scheme, the convective flux and chemical source terms are treated implicitly, whereas the viscous terms are treated explicitly. The LU scheme only requires the scalar diagonal inversion for the flow equations (i.e. momentum equations and energy equations) and the diagonal block inversion for the species equations. As a result, the LU scheme has the advantage of a fast convergence rate while requiring the computational cost similar to that of an explicit scheme, and therefore is particularly attractive for reacting flows with large chemical species systems.

In the following, for simplicity, the derivation of the LU will be presented for the Euler equations. A prototype implicit scheme for a system of nonlinear hyperbolic equations such as the Euler equations can be formulated as:

$$\tilde{U}^{n+1} = \tilde{U}^n - \beta\Delta t\left\{D_\xi \tilde{F}\left(\tilde{U}^{n+1}\right) + D_\eta \tilde{G}\left(\tilde{U}^{n+1}\right)\right\} - (1-\beta)\Delta t\left\{D_\xi \tilde{F}\left(\tilde{U}^n\right) + D_\eta \tilde{G}\left(\tilde{U}^n\right) - \tilde{S}\left(\tilde{U}^n\right)\right\}$$

Let the Jacobian matrices are

$$\tilde{A} = \frac{\partial \tilde{F}}{\partial \tilde{U}}, \qquad \tilde{B} = \frac{\partial \tilde{G}}{\partial \tilde{U}}, \qquad \tilde{Z} = \frac{\partial \tilde{S}}{\partial \tilde{U}}$$

and the correction

$$\delta\tilde{U} = \tilde{U}^{n+1} - \tilde{U}^n$$

thus, the scheme can be linearized by setting

$$\tilde{F}\left(\tilde{U}^{n+1}\right) = \tilde{F}\left(\tilde{U}^n\right) + \tilde{A}\delta\tilde{U}$$
$$\tilde{G}\left(\tilde{U}^{n+1}\right) = \tilde{G}\left(\tilde{U}^n\right) + \tilde{B}\delta\tilde{U}$$
$$\tilde{S}\left(\tilde{U}^{n+1}\right) = \tilde{S}\left(\tilde{U}^n\right) + \tilde{Z}\delta\tilde{U}$$

then the equations can be written as

$$\left\{I + \beta\Delta t\left(\tilde{A}^+_{i,j} - \tilde{A}^-_{i,j} + \tilde{B}^+_{i,j} - \tilde{B}^-_{i,j} - \tilde{Z}\right) + \beta\Delta t\left(\tilde{A}^-_{i+1,j} + \tilde{B}^-_{i,j+1}\right) - \beta\Delta t\left(\tilde{A}^+_{i-1,j} + \tilde{B}^+_{i,j-1}\right)\right\}\delta\tilde{U} = -\Delta t RHS$$

which can be symbolically expressed as

$$(D + L + U)\delta\tilde{U} = \Delta t RHS \tag{1}$$

where

$$D = I + \beta\Delta t(r_{\tilde{A}} + r_{\tilde{B}}) - \beta\Delta t\tilde{Z}$$
$$L = -\beta\Delta t\left(\tilde{A}^+_{i-1,j} + \tilde{B}^+_{i,j-1}\right)$$
$$U = \beta\Delta t\left(\tilde{A}^-_{i+1,j} + \tilde{B}^-_{i,j+1}\right)$$

The left-hand side of Eq. (1) can be approximately factored into the product of two operators:

$$(D + L)D^{-1}(D + U)\delta\tilde{U} = -\Delta t RHS$$

So, this scheme can be implemented in the following sequence:

$$(D + L)\delta\tilde{U}^* = -\Delta t RHS$$
$$(D + U)\delta\tilde{U} = D\delta\tilde{U}^*$$
$$\tilde{U}^{n+1} = \tilde{U}^n + \delta\tilde{U}$$

4. Chemistry kinetic model

In the present study, three different chemical reaction models, including Hydrogen/Oxygen, Kerosene/Oxygen and $CH_3N_2H_3/N_2O_4$ reactions, are developed for the nozzle flow computations. In different cases, the species and the reactions in the computational code are specified according to the oxidizer and the fuel used. The follows are the C–H–O–N reaction model, which has 12 species and all the 14 reactions, and the model of Kerosene/Oxygen reaction has the first 9 reactions (marked with $*$ and $**$), and the first 8 reactions (marked with $*$) for the Hydrogen/Oxygen reaction model.

$H_2 + M \Leftrightarrow 2H + M$	$*$
$O_2 + M \Leftrightarrow 2O + M$	$*$
$H_2O + M \Leftrightarrow H + OH + M$	$*$
$OH + M \Leftrightarrow O + H + M$	$*$
$H_2O + O \Leftrightarrow 2OH$	$*$
$H_2O + H \Leftrightarrow OH + H_2$	$*$
$O_2 + H \Leftrightarrow OH + O$	$*$
$H_2 + O \Leftrightarrow OH + H$	$*$
$CO + OH \Leftrightarrow CO_2 + H$	$**$
$O + N_2 \Leftrightarrow N + NO$	$***$
$H + NO \Leftrightarrow N + OH$	$***$
$O + NO \Leftrightarrow N + O_2$	$***$
$NO + OH \Leftrightarrow H + NO_2$	$***$
$NO + O_2 \Leftrightarrow O + NO_2$	$***$

A set of n_r reactions between n_s species can be described by

$$\sum_{i=1}^{n_s} V_{ij}^f R_i \Leftrightarrow \sum_{i=1}^{n_s} R_i, \quad j = 1, 2, \ldots, n_r$$

where v_{ij}^f and v_{ij}^b are the stoichiometric coefficients of species i for the forward and backward reaction j respectively, and R_i is the molar concentration of species i. The reaction rate constant for the forward and backward reaction is given by the Arrhenius formular:

$$k_i^f = A_{fi} T^{B_{fi}} \mathrm{e}^{-C_{ft}/T}$$
$$k_i^b = A_{bi} T^{B_{bi}} \mathrm{e}^{-C_{bt}/T}$$

where the values of coefficients of reaction rates are listed in Ref. [2].

The rate of production for species i is:

$$\dot{\omega}_i = M_i \sum_{j=1}^{n_r} (v_{ij}^b - v_{ij}^f) \left(\frac{\rho}{\bar{M}}\right)^n \times \left[k_j^f \prod_{l=1}^{n_s} \left(\frac{\rho_l}{M_l}\right)^{v_{jl}^f} - k_j^b \prod_{l=1}^{n_s} \left(\frac{\rho_l}{M_l}\right)^{v_{jl}^b} \right]$$

5. CFD-based optimization

In this work, an existing nozzle design that has been used in practical activity is chosen, which is then optimized using the CFD code coupled with an optimizer to look for improvements in the thrust.

The objective function is:

$$\mathrm{Obj}(X) = \int_0^{A_{\mathrm{exit}}} (\rho u^2 + p)\, \mathrm{d}A$$

where ρ, u, p and A are local density, axial velocity, pressure, and cross-sectional area respectively. For a rocket nozzle, $\mathrm{Obj}(X)$ is defined as the vacuum thrust which is to be maximized to obtain an optimum nozzle design.

The design variables X are usually coefficients used to define a wall boundary or quantities that specify the flow-field conditions. For a nozzle design, the flow conditions are usually given, and the wall contour must be determined. In this work, the length and area ratio are specified, and the cubic function is used to describe nozzle wall contour downstream of the throat. There are 7 controlling points to determine the shape of nozzle wall, whose positions are shown in Fig. 1. And the X are the wall radii at these points. The cubic spline interpolation is used in each of the intervals of these points as well as the other two fixed points of the wall at throat and nozzle exit. So, the resulting function to describe nozzle wall contour downstream of the throat is twice continuously differentiable.

Three optimization algorithms are used in the present study: one is the successive quadratic programming (SQP) method. Another is the genetic algorithm (GA). The third algorithm is the interdigitation strategy, which combines multiple optimization algorithms to explore their desirable aspects for solving

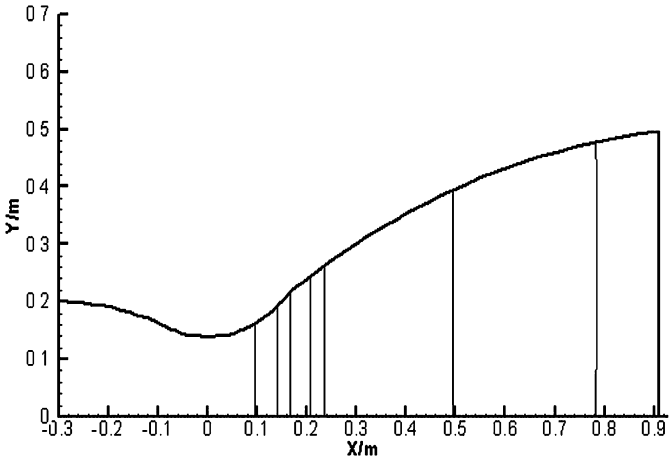

Fig. 1. Positions of controlling points of nozzle contour.

complex problems. For this problem with a high degree of nonlinearity and expected numerous local optima, an exploratory technique such as the genetic algorithm is initially applied to conduct a global search of the design space to identify regions in which the best solutions may lie. Then a sequential quadratic programming technique is applied, starting from the solutions obtained from the exploratory search, to conduct a more local search to identify the best solution in the region of interest. This so-called interdigitation of optimization techniques can be fully automated with the engineering software of iSIGHT [6].

6. Results and discussions

The ability of the code to compute nozzle flows is assessed by computing three nozzles, namely nozzles A, B and C, for which both experimental data and previous numerical results are available for comparison.

Results of nozzle A are presented as planar nozzle reported by Mason et al. [5]. The geometrical details for this test case are given in Fig. 2. Computations have been performed using both the Navier–Stokes equations and the Euler equations. The pressure distribution on the centerline and the wall are compared with the experimental data. Figs. 3 and 4 show the solution of the Euler equations. The numerical results and the experimental data are in a good agreement either on the centerline positions and on the nozzle wall. Figs. 5 and 6 show the solution to the Navier–Stokes equations. Again, the agreement between the numerical results and the experimental data is very good, and better than what is presented in Ref. [3]. By comparing

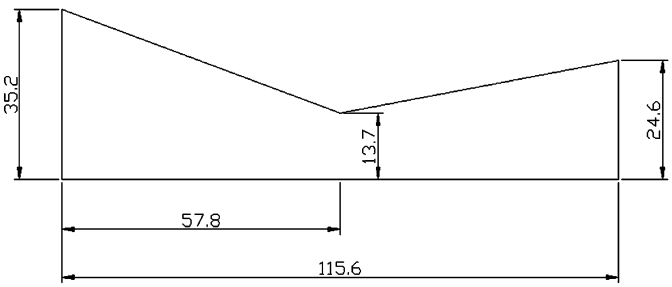

Fig. 2. Planar converging-diverging nozzle (dimensions in mm).

Figs. 4 and 6, it can be seen that the NS solution gives slightly better pressure distributions on the centerline and the wall.

Fig. 7 shows the pressure and temperature contours of nozzle B which is relatively large in size. The fuel of nozzle B is Kerosene, and the oxidizer is Oxygen. Fig. 8 shows the contours of nozzle C which is small in size. The propellants of nozzle C are $CH_3N_2H_3$ and N_2O_4. Table 1 shows the comparison of nozzle performance predicted by CFD code and the experimental data. Both of the calculations are performed with chemical non-equilibrium Navier–Stokes equations.

From these test cases, it can be concluded that the CFD code used in this work is an eligible flow solver and applicable for the analysis and optimization of liquid rocket engine nozzle, whether it is a small nozzle or a large one.

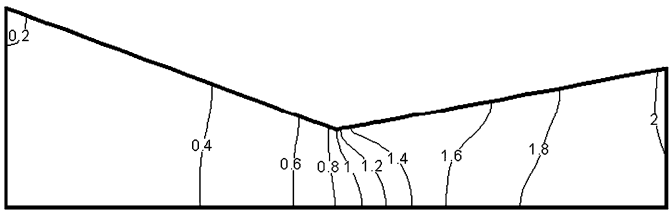

Fig. 3. Isomach lines for the inviscid case.

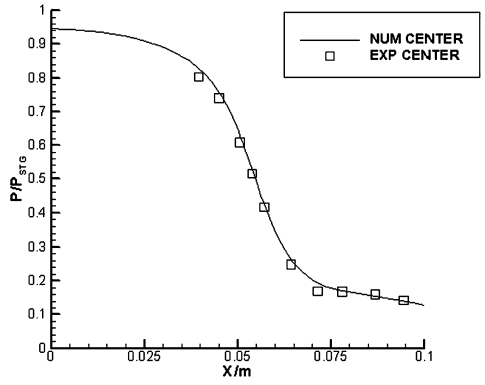

(a)

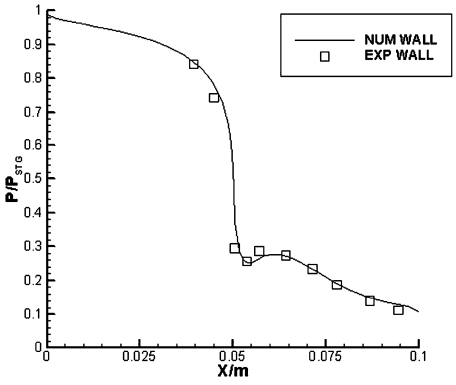

(b)

Fig. 4. Pressure distribution predicted by Euler equations. (a) On the centerline. (b) On the wall.

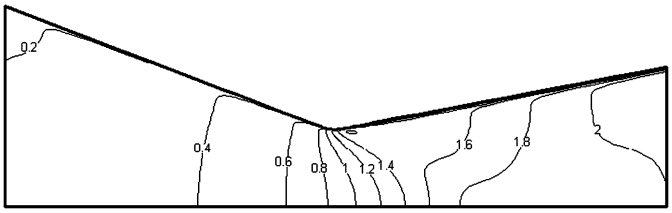

Fig. 5. Isomach lines for the viscous case.

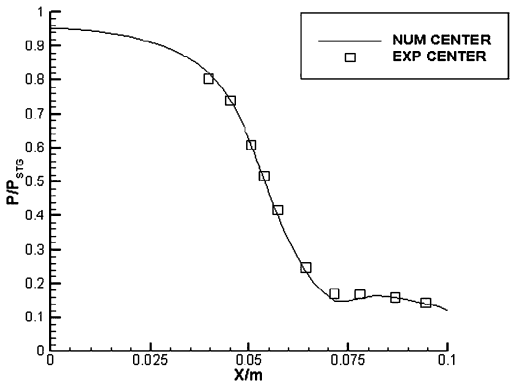

(a)

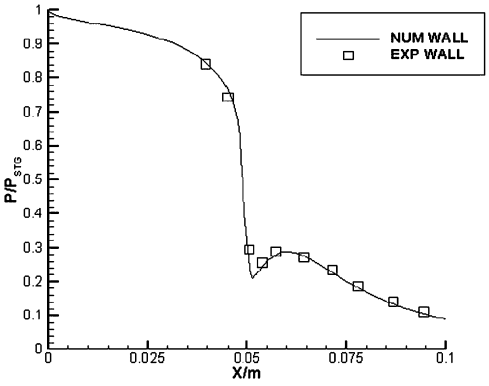

(b)

Fig. 6. Pressure distribution predicted by NS equations. (a) On the centerline. (b) On the wall.

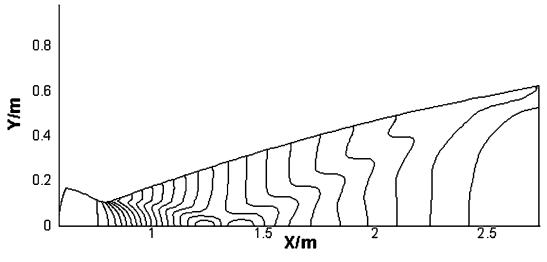

(a)

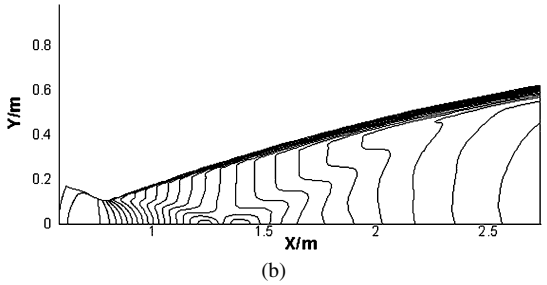

(b)

Fig. 7. Numerical computational contours of nozzle B. (a) Pressure contour. (b) Temperature contour.

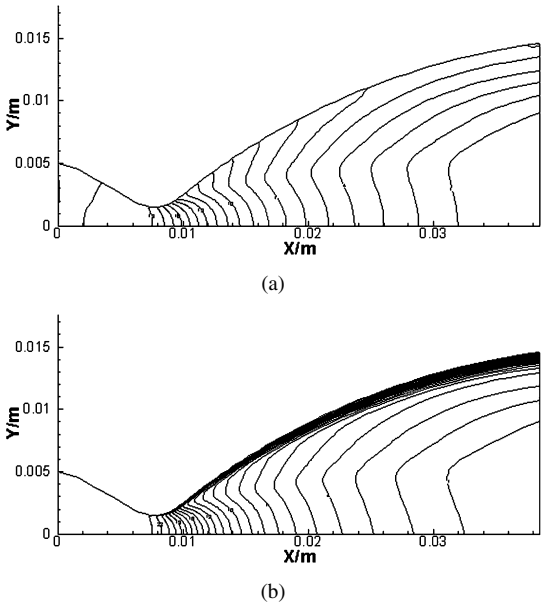

Fig. 8. Numerical computational contours of nozzle C. (a) Pressure contour. (b) Temperature contour.

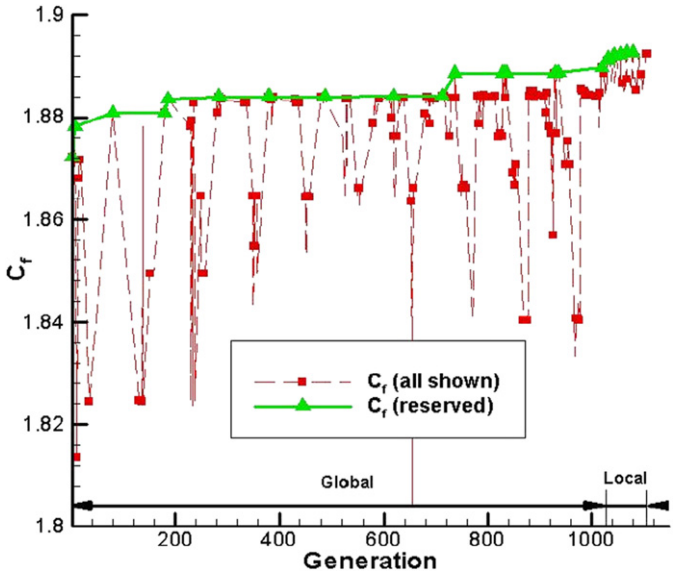

Fig. 9. Evolution history of interdigitation strategy.

Thus, the CFD code, considering the axisymmetric N–S equations and chemical reactions, is then applied to design axisymmetric rocket engine nozzle. The results obtained by three different optimization algorithms are shown in Table 2. The genetic algorithm and interdigitation method generated almost the same optimization results, while the successive quadratic programming method failed to find the global maximum value and only a local optimal result is obtained.

Fig. 9 shows the evolution history of interdigitation strategy. The optimization process began from a global search in order to explore the solution space in a more efficient manner. The global search lasted until the whole solution space had been examined and a sub-zone, the optimal solution might lie, had been located. Then a local search was started in the sub-zone until the optimal solution had been found. Wild oscillation can be observed in the optimization process, especially in the global searching phase. According to the demand of genetic algorithm, used for global optimization, only the individuals better than the previous ones are preserved and the worse ones are discarded. The results of interdigitation strategy will be used for further discussions in the following context.

Table 1
Comparisons of vacuum thrust coefficient

	Numerical result	Experimental data	Error
Nozzle B	1.88	1.92	2.08%
Nozzle C	1.81	1.77	2.26%

The computed pressure contour for the initial nozzle and optimized nozzle are shown in Fig. 10. For the optimized nozzle, a more weak compression wave (induced by the not-smooth-enough connection of contour) and a more uniform parameter distribution on the nozzle exit plane can be observed, which are favorable for the performance improvement.

In order to compare the performance of the optimized nozzle with the initial one, different computational cases are performed to demonstrate the reason for the performance improvement by using different computational models, which include one-dimensional reaction flow, two-dimensional inviscid frozen flow, two-dimensional viscous frozen flow, two-dimensional inviscid reaction flow and two-dimensional viscous of reaction flow. Performances predicted by different models indicate different mechanism of losses. For example, the difference between the performances obtained by Euler and NS models indicates the viscous (friction) loss in the nozzle.

For the optimized nozzle and initial nozzle, different computations are performed. The comparison of vacuum thrust coefficients of different computational cases are shown in Fig. 11. In the present work, the thrust coefficient is defined by

$$C_f = \frac{F}{P_c A_t}$$

where P_c is the combustor pressure and A_t is the nozzle throat area.

In Fig. 11, the nozzle performances predicted by different computational models are given in order to illustrate effects of the models on the performances. It can be seen that the performances of the optimized nozzle predicted by different models

Table 2
Results of different optimization methods

Method	Initial vacuum thrust coefficient	Optimized vacuum thrust coefficient	Improvement
Successive quadratic programming	1.865	1.880	0.804
Genetic algorithm	1.865	1.893	1.501
Interdigitation strategy	1.865	1.892	1.448

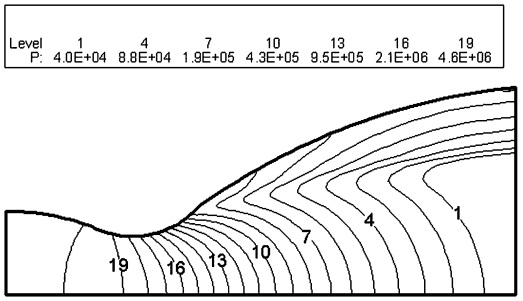

(a)

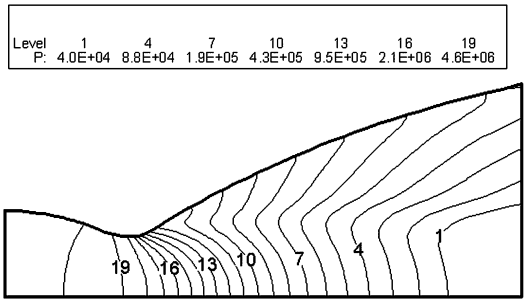

(b)

Fig. 10. Pressure contours in nozzles obtained by NS solver (unit: Pa). (a) Initial nozzle. (b) Optimized nozzle.

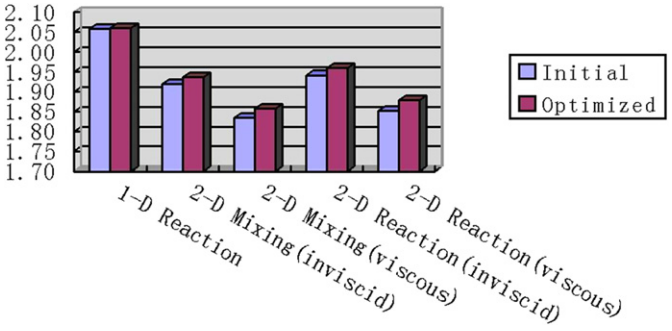

Fig. 11. Comparison of vacuum thrust coefficients of different cases.

are better than that of the original one. In addition, the results of one-dimensional case is better than that of the two-dimensional case, inviscid case better than viscous case, reaction case better than mixing case when other factors keeps the same.

Several different performance losses are defined to analyze the detail of performance improvement of the optimized nozzle. They are friction loss, chemically frozen loss and axial loss.

Friction Loss coefficient is defined as

$$\zeta_f = \frac{C_{fE} - C_{fN}}{C_{fE}} = \frac{\Delta C_f}{C_{fE}}$$

where C_{fN} and C_{fE} are the vacuum thrust coefficients obtained by solving the N–S and Euler equations respectively. The comparisons of friction losses are shown in Table 3. For the optimized nozzle, the friction loss is less than that of initial nozzle in both mixing (non-reaction) and reaction cases.

In this paper, the Chemically Frozen Loss is defined as:

$$\zeta_n = \frac{C_{fr} - C_{fm}}{C_{fm}} = \frac{\Delta C_f}{C_{fm}}$$

Table 3
Comparisons of friction losses

		Initial nozzle			Optimized nozzle		
		C_{fE}	C_{fN}	ζ_f	C_{fE}	C_{fN}	ζ_f
Friction losses	Mixing	1.932	1.847	4.4%	1.950	1.871	4.0%
	Reaction	1.956	1.865	4.7%	1.974	1.893	4.1%

Table 4
Comparisons of chemically frozen losses

		Initial nozzle			Optimized nozzle		
		C_{fm}	C_{fr}	ξ_n	C_{fm}	C_{fr}	ξ_n
Chemically frozen losses	Euler	1.932	1.956	1.2%	1.950	1.974	1.2%
	N–S	1.847	1.865	1.0%	1.871	1.893	1.2%

Table 5
Comparisons of axial losses

	Initial nozzle			Optimized nozzle		
	C_{fo}	C_{ft}	ξ_x	C_{fo}	C_{ft}	ξ_x
Axial losses	2.074	1.956	5.7%	2.076	1.974	4.9%

where C_{fr} is the vacuum thrust coefficient obtained by considering the chemical reaction in the nozzle, and C_{fm} is the vacuum thrust coefficient if the flow in the nozzle is frozen. The comparisons of chemically frozen losses are shown in Table 4. It seems that the contour optimization does not generate obvious performance improvement on the chemical reaction aspect.

Axial Loss coefficient is defined as:

$$\zeta_x = \frac{C_{fo} - C_{ft}}{C_{fo}} = \frac{\Delta C_f}{C_{fo}}$$

where C_{fo} is the vacuum thrust coefficient obtained by solving the one-dimensional Euler equations, and C_{ft} is the vacuum thrust coefficient obtained by solving the two-dimensional Euler equations. The comparison of axial losses is shown in Table 5. It can be seen that by nozzle contour optimization, the axial loss is obviously reduced.

7. Conclusion

The computational fluid dynamics method is coupled with the optimization process in order to predict the nozzle performance more accurately. The CFD-based optimization procedure achieved better nozzle performance than the initial one. Although the chemically frozen loss does not show promotion obviously before and after optimization, friction loss and axial loss decrease. The optimization generates nearly 1.5% performance improvement over the initial one, approximately half of which is attributed to the decrease of friction loss, and the other half to the decrease of axial loss.

References

[1] G. Candler, J. Perkins, Effects of vibrational nonequilibrium on axisymmetric hypersonic nozzle design, AIAA Paper 91-0297, 1991.

[2] J.S. Evans, C.J. Schexnayder Jr., Influence of chemical kinetics and unmixedness on burning in supersonic hydrogen flames, AIAA Journal 18 (1980) 188–193.
[3] K.C. Karki, S.V. Atankar, Pressure based calculation procedure for viscous flows at all speeds in arbitrary configurations, AIAA Journal 18 (1989) 1167–1174.
[4] S. Kim, Calculations of low Reynolds number rocket nozzles, AIAA Paper 93-0888, 1993.
[5] M.L. Mason, L.E. Putnam, R.J. Re, The effect of throat contouring on two-dimensional converging-diverging nozzles at static conditions, NASA-TP-1704, 1980.
[6] N.K. Patrick, J.P. Evans, D. Powell, Interdigitation for effective design space exploration using iSIGHT, Journal of Structural and Multidisciplinary Optimization 23 (2002) 111–126.
[7] G.V.R. Rao, Exhaust nozzle contour for optimum thrust, Jet Propulsion 28 (6) (1958).
[8] J.S. Shuen, Upwind differencing and LU factorization for chemical non-equilibrium Navier–Stokes equation, Journal of Computational Physics 99 (1992) 233–250.
[9] S. Yoon, A. Jameson, Lower-upper symmetric-Gauss–Seidel method for the Euler and Navier–Stocks equations, AIAA Journal 26 (1988) 1025–1026.